Research Article

Extracting voltage-dependent series resistance of single diode model for organic solar cells

Ali Khorami[1] · **Mojtaba Joodaki**[2]

Abstract

In this paper, a modified equivalent circuit model is proposed to elucidate the electrical behavior of Organic Solar Cells (OSCs). In this way, this single diode model uses a voltage-dependent series resistance to enhance the modeling accuracy while benefiting from the simplicity of the equivalent circuit. The voltage dependency of the series resistance of OSCs is mainly related to internal processes of charge extraction and charge transport. The charge extraction at electrodes is influenced by space charge effect and many other physical parameters including exciton lifetime, dissociation rate, and free carrier recombination.The carrier transport process from donor/acceptor interface to electrodes is governed by its mobility. On the other hand, carrier mobility of organic material depend on field variation. The voltage-dependent series resistance is not often used in the today's OSC circuit models due to a lack of a reliable field-dependent extraction approach. This proposed model expands its application in finding optimum bias, behavior analysis and efficiency improvement of OSCs. At first, a genetic algorithm curve fitting is applied to the measured current–voltage characteristics to extract the model's parameters assuming an average constant series resistance. Then a new algorithm is proposed for extracting the voltage-dependent series resistance. Finally, consistency of the extracted field dependent series resistance with previous literature is presented. The results shows that the average mean square errors of the predicted J–V characteristics by the proposed approach for five cells under test is improved by a factor of 10^6 in comparison with those of a constant value R_s approach. This is the first successful extraction of voltage dependent series resistance of OSCs from DC current–voltage characteristic.

✉ Mojtaba Joodaki, Joodaki@um.ac.ir; Ali Khorami, ali.khorami@stu.um.ac.ir | [1]Department of Electrical Engineering, Khorasan Institute of Higher Education, Mashhad, P.O. Box: 91775-1111, Iran. [2]Department of Electrical Engineering, Faculty of Engineering, Ferdowsi University of Mashhad, Mashhad, P.O. Box: 91775-1111, Iran.

SN Applied Sciences (2019) 1:619 | https://doi.org/10.1007/s42452-019-0613-2

Received: 24 September 2018 / Accepted: 14 May 2019 / Published online: 22 May 2019

Graphical abstract

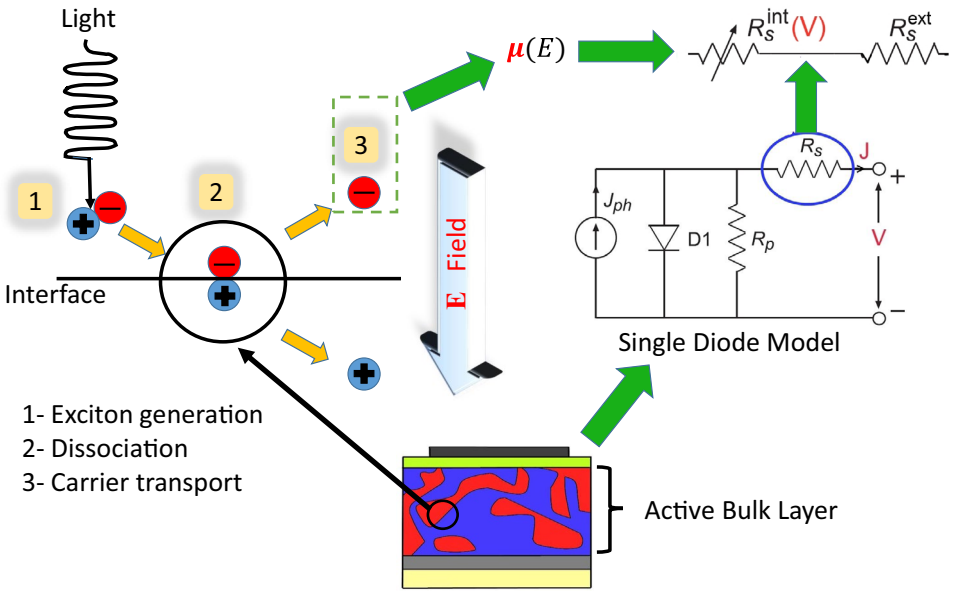

Keywords Voltage-dependent · Series resistance · Parameters extraction · Bulk heterojunction · Organic solar cell

1 Introduction

Organic photovoltaic cells (OPCs) represent a highly attractive candidate for harvesting solar energy because of promising properties such as mechanical flexibility, low cost fabrication, light weight, ease of processability and semi-transparency [1, 29]. The single junction bulk hetrojunction (BHJ) organic solar cells (OSCs) have reached power conversion efficiencies (PCE) surpassing 11% [21], however, further electrical performance and reliability improvements are required. In recent years, promising OSCs with non-fullerene acceptors (NFAs) has also been introduced [12]. In comparison with OSCs with fullerene acceptors, NFAs provide larger power conversion efficiency (14% for single junction and 18% for tandem cells), excellent stability and tunability of bandgaps, energy levels, crystallinity and planarity. Usually, electrical simulation and modelling are performed prior to solar cell installation in order to optimize the performance of the overall system.

The physical modeling required for exciton and carrier transport studies is often performed with differential equations [30, 48]. These equations can be numerically solved by discretization methods including finite difference method [23] or meshless methods such as chebichef function method [15]. Solving these models results in predicting the behavior of organic solar cell and achieving all information at each point inside the device [8, 31]. In photovoltaic system design, a simulation with low computational burden is needed to predict the module performance and consequently to optimize the power output. Therefore, an equivalent circuit model elucidating the electrical behavior of OSCs is of vital interest [28].

Equivalent circuit models of OSCs are both simple and fast. They are also very useful for understanding how different factors influence on the behavior of solar cells [2, 11, 36]. The models simplicity limits the fitting quality (the process that fits the models parameters to the measured I–V curve). Therefore, the equivalent circuit models are often used possess additional or modified elements [2, 11, 17, 19, 26, 32–34, 36, 46, 50]. The single diode model based on Shockley relation, shown in Fig. 1, is often employed for modeling organic/inorganic solar cells [5, 43]. The equivalent circuit implements the Shockley relationship as:

$$J = J_0\left(exp\left(\frac{V - JR_s}{nV_t}\right) - 1\right) + \frac{V - JR_s}{nV_t} - J_{ph} \quad (1)$$

where J is the current density, V is cell voltage, J_{ph} is generated photocurrent,J_0 is the saturation current density under reverse bias, R_p is the parallel or shunt resistance, R_s is the series resistance, V_t is the thermal potential and n is the ideality factor.

In this paper, we proposed a new equivalent circuit with a voltage-dependent series resistance based on Eq. (1). This voltage-depended series resistance reflects the field

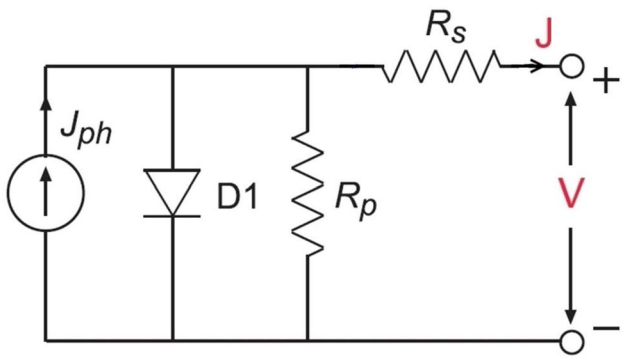

Fig. 1 The typical single diode model

dependency of the organic materials. In this paper, voltage dependency of the series resistance is explained using a simple expression, see Eq. (10). Different approaches have already been suggested for extraction of series resistance [37]. For example, R_s can be extracted from the slope of the dark current–voltage curve (at voltages higher than the open circuit voltage) [37] or if we consider a voltage independent photocurrent, we can extract the R_s from the slope of $J\frac{dV}{dJ}$ versus J [57]. In another method a closed form relation is given to extract the R_s at open circuit bias [9]. Though, these methods have their own advantages and shortcomings, none of them is suitable for extraction of the voltage-dependent series resistance. In this paper, a numerical algorithm is proposed for extraction of $R_s(V)$ which in fact is an extension to the method in [37]. Other parameters of the equivalent circuit are also extracted employing an intelligent optimization method. The multi junction OSCs would be modeled with multi-diodes equivalent circuits. Although in this work we focused on modeling single-junction cells, basically our model can be extended for multi-junction cells, too.

The rest of paper is organized as follows. In Sect. 2, a basic of series resistance in OSC and the algorithm implemented for the conventional parameters extraction are described. In Sect. 3, after obtaining an analytical equation to calculate the voltage-dependent at open circuit voltage (V_{oc}), the voltage-dependent extraction approach for other bias points is explained and two verification criteria are given. In Sect. 4, the new method for variable series resistance is explained. In Sect. 5 proposed method is applied to the measured J–V curves and the results are discussed. Finally, the conclusion is presented.

2 Series resistance model

The series resistance (R_s), which is influenced by charge carrier mobility (μ_n and μ_p), is one of the key parameters that affects the electric performance of OSC in terms of fill factor (FF) [62] and the mobility is affected by traps or other barriers (hopping) [5, 25]. Also, dense photocarriers around the electrode of OSC, because of difference between carrier mobilities, results in space charge accumulation (limit) and degradation of electrical properties such as the series resistance. Several analytical and numerical approaches have been proposed to obtain the accurate value of series resistance [4, 9, 10, 16, 27, 35, 37, 41, 42, 45, 51, 61, 62] , however, few of them focused on the voltage dependency of series resistance [22, 27, 40, 62]. Since any rising in R_s reduces efficiency of the cell, many researchers tried either to use suitable materials [59] or develop better manufacturing technologies [24] to reduce it. Both of these groups need more accurate models for better understanding and designing OSCs. R_s is basically determined by charge mobility; however, other phenomena, such as space charge limitation and traps, have strong influences on it as well. Series resistance (R_s) of a typical OSCs is showed in Fig. 2, consists of two parts including external part and internal part as:

$$R_s = R_s^{ext} + R_s^{int} \tag{2}$$

The external part (R_s^{ext}) is usually considered as a constant value and consist of the contacts resistance (R_{elec}) and buffer layers (R_{buff}).

$$R_s^{ext} = R_{elec} + R_{buff} \tag{3}$$

Usually one of the contacts is made with Aluminium or silver that has large conductivity, hence its series resistance is negligible. But the other contact commonly is made with ITO or FTO that has higher resistance. Assuming lateral current flow, the ITO series resistance (R_{elec}) is [47]:

$$R_{elec} = \frac{W^2}{3\sigma_{elec}t_{elec}} \tag{4}$$

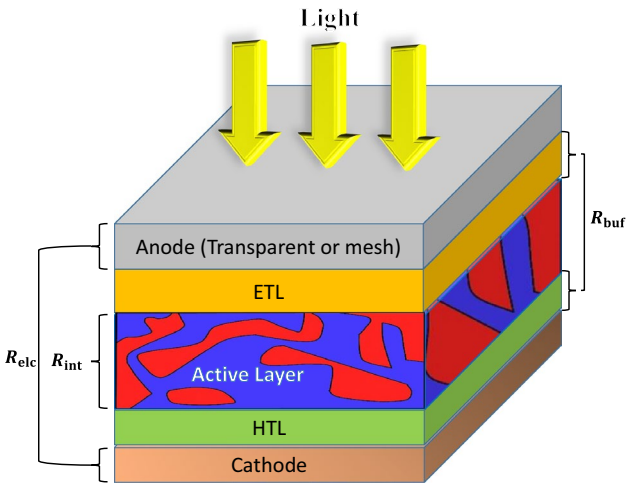

Fig. 2 Schematic structure of the five cells under test

where W is device width (in our case 3 mm), is anode thickness and is anode contact conductivity. The series resistance of all other layers is the ratio of their thickness over electric conductivity.The 1 nm LiF layer (as buffer) has series resistance of about 1 ΩCm^{-2} [60] and for thin buffer layer it is negligible.

In the bulk heterojunction OSCs, the internal part of series resistance (R_s^{int}) is mainly affected by the active layer carrier transport and traps and defects at interfacial boundaries [22]. The main idea behind variable is that charge carrier mobility in organic material varies as a function of the electrical field. The charge carrier mobility in organic materials obeys the Poole–Frenkle relationship [13],

$$\mu(E) = \mu_0 exp\left(\gamma \cdot E^{0.5}\right) \tag{5}$$

where E is the electric field, μ_0 is the zero field mobility and γ is the Poole–Frenkle constant which is determined as [48]:

$$\gamma = \frac{q^{0.5}}{2v_T\sqrt{\pi\varepsilon_0\varepsilon_r}} \tag{6}$$

where ε_0 is the vacuum permittivity, ε_r is the material permittivity, T is the temperature and K_B is the Stefan–Boltzmann constant. Similarly for active layer resistance we have:

$$R_{int} = \frac{L_{active}}{\sigma_{active}A} \tag{7}$$

when Electrical conductance of active layer is illustrated as Eq. (8):

$$\sigma_{active} = q\left(n\mu_n + p\mu_p\right) \tag{8}$$

For applying these equations for calculating resistance of active layer, electrical field distribution is needed. The electrical field is related to applying voltage to the electrodes of cell. The modified drift-diffusion model is used for determining voltage distribution in BHJ solar cell [30]. Figure 3 shows the result of this simulation. In this figure, one dimensional inside voltage distribution of the simulated organic solar cell is illustrated. It shows this distribution is approximately linear except near contacts. Thus we can suppose the distribution of inside potential is linear as:

$$V_{app} = ax + b \tag{9}$$

where, x is axis that perpendicular to the surface cell. Factors a and b are determined according to boundary conditions. At this simulation linear regression determine a = − 0.01 and b = 0.61. Since electrical field is resulted by voltage derivation, it can be inferred E = a. Relations (5)–(8) and E=a lead to Eq. (10) that used for finding series resistance in active layer.

$$R_{int} = \frac{L_{active}}{q\left(n\mu_{0n} + p\mu_{0p}\right)exp\left(\gamma \cdot a^{0.5}\right)} \tag{10}$$

Also, dependency of series resistance to applying bias variation can be influenced by the space charge. The space charge limit effect is a universal phenomenon in semiconductor devices and also sets a fundamental electrostatic limit in electrical properties of organic semiconductor devices with unbalanced photocarriers mobility and high exciton generation efficiency [3, 39, 49, 53]. Photo current and series resistance may take effect of this phenomena but it is not inspected in this paper. Considering Eqs. (2) to (10), the voltage dependency of the series resistance is obvious.

3 Modeling J–V curve

Considering a field-dependent series resistance in OSC equivalent circuit improves the accuracy of the model. In this paper we propose a method for extracting a voltage-dependent series resistance from current–voltage (J–V)

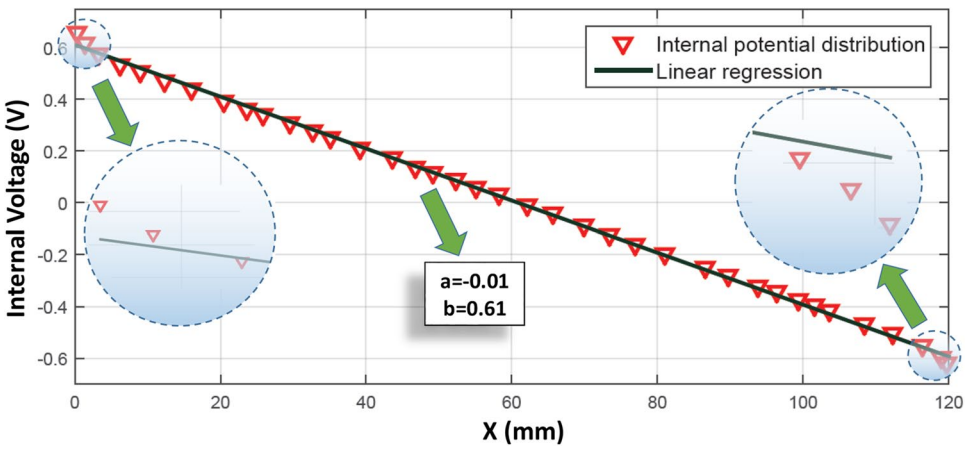

Fig. 3 Distribution of internal voltage

characteristics. This method can be applied to both dark and illuminated measured J–V curves. However, due to light intensity dependency of OSC parameters [52, 54], an illuminated J–V curves is more realistic and it is preferred for extraction in our work.

Charles et al. [9] presented a practical method of extracting single diode equivalent circuits parameters, including constant value series resistance, from J–V characteristics. Jain and his coworker [25] used the Lambert W-function for a similar purpose. In another effort, an analytical method is developed to calculate the parameters of the solar cells using Trans Function Theory [51]. In this work, we have employed an artificial intelligent fitting algorithm based on a genetic algorithm to extract J_0, R_p, n and J_{ph} from measured J–V curves. The population is considered equal to 50 chromosomes (it is not critical, and the population size has effect on convergence time) and mean square error (MSE) is used as fitness (objective) function:

$$MSE = \frac{1}{P}\sum_{k=1}^{P}\left(J_k^{Mes} - J_k^{Cal}\right) \tag{11}$$

where P denotes number of measured current density points and J_k^{Mes} and corresponding J_k^{Cal} show the measured and the calculated current density at each measurement point, respectively. Equation (1) is used for calculating J_k^{Cal} in each generation based on the extracted parameters in that generation.

In this fitting algorithm (GA), in addition to above mentioned parameters, a constant value R_s, so called R_s^{GA}, is also extracted. On the other hand, the simplest method to find approximated value of the series resistance is obtained from the voltage–current differentiation at open circuit voltage as below:

$$R_s^{op} = \frac{dV}{dJ}|_{V=V_{oc}} \tag{12}$$

In fact, R_s^{op} is the dynamic resistance at open circuit voltage. However, some other researchers prefer to derive the series resistance at maximum power (operation point), as below [11]:

$$R_s^{mp} = \frac{dV}{dJ}|_{V=V_{mp}} \tag{13}$$

One can also obtain the series resistance at large bias voltages as:

$$R_s^{\infty} = \frac{dV}{dJ}|_{V=\infty} \tag{14}$$

4 Voltage dependent series resistance extraction

Prior to extracting voltage-dependent series resistance, it should be noted that in some OSCs, an S-shaped deformation or S-kink emerges within the fourth quadrant of the measured J–V characteristics. In OSCs, the S-kinks origin has been attributed to various physical phenomena such as charge accumulation at the cathode interface [14], the presence of strong interface dipoles [20], unbalanced charge transport and interfacial energy barriers [7]. Both S-kink and voltage-dependent photocurrent can also be caused by space charge limitation (SCL) [58], interfacial energy barriers shifting and charge transport dissociation and recombination [38]. In order to model these phenomena a voltage-dependent current source or additional diodes should be included in the model [18]. The presence of such a bend in J–V curve reduces the solar cell's fill factor seriously and thus represents a reduction in the cell's power conversion efficiency. Thus, usually these effects are avoided, minimized or shifted using suitable materials selection and modification of the fabrication processes [14, 44, 56]. Therefore, a constant value photocurrent is considered in our model.

If a voltage dependent series resistance is assumed, from Eq. (1), we can drive $\frac{d}{dJ}$ as follows:

$$1 = -\frac{dJ_{ph}}{dJ} + J_0 exp\left(\frac{V - JR_s}{nV_t}\right)\left(\frac{1}{nV_t} + \frac{1}{R_p}\right) \times \left(\frac{dV}{dJ} - R_s - J\frac{dV}{dJ}\cdot\frac{dR_s}{dV}\right) \tag{15}$$

Considering Eqs. (12) and (15), R_s^{oc} at the open circuit voltage ($J = 0$ and $V = V_{oc}$) is:

$$R_s^{oc} = R_s^{op} - \frac{1}{\frac{J_0}{nV_t}exp\left(\frac{V_{oc}}{nV_t}\right) - \frac{1}{R_p}} \tag{16}$$

In which R_s^{op} and V_{oc} can be easily obtained from measure J–V curves, however, J_0, n and R_p are achieved using the genetic algorithm method as discussed in previous section. If series resistance varies with changing bias voltage, then analytical relation cant be received. So, relation (16) is acceptable only in open circuit voltage.

In (1), if $R_s << R_p$ (where, R_p is typically more than several orders of magnitude larger than R_s), $\frac{J}{J_0} >> 1$(this approximation holds only for forward biases)and $\acute{J} = J - J_{ph}$ we can write:

$$\Longrightarrow \acute{J} = J_0 \cdot \left(exp\left(\frac{V - JR_s}{nV_t} \right) - 1 \right)$$
$$\Longrightarrow \frac{\acute{J}}{J_0} + 1 = exp\left(\frac{V - JR_s}{nV_t} \right) \quad (17)$$
$$\Longrightarrow \frac{V - JR_s}{nV_t} \cong \ln\left(\frac{\acute{J}}{J_0} \right)$$

And differentiation of the above equation gives ($d\acute{J} = dJ$):

$$\acute{J}\frac{dV}{dJ} \cong \cdot R_s \cdot J + nV_t \quad (18)$$

In Eq. (18) one can draw $\acute{J}\frac{dV}{dJ}$ as a function of J, then the slope will represent the extracted R_s. We should remember that J_{ph} is already extracted using the proposed GA algorithm. In the event of a constant R_s a regression is usually used for calculation of the slope. But if R_s is voltage dependent, the slope is a function of applied voltage. Therefore, in our method, the regression process is applied to the measured data over a limited voltage window for each bias point (V_i). This approach is called Window Regression Algorithm (WRA) and it is explained as below:

$$R_s^{var}(V_i) = m\left(\acute{J}\frac{dV}{dJ}, J \right)|_{V=V_i} \quad (19)$$

where, m denotes slope. The window regression width is limited to $2N + 1$measured data around the desired extraction point. For example, the Fig. 4 illustrates the window regression results around V_i with $N = 10$. The extracted R_s^{var} at $V_i = 0.55V$ is 48 ohms. In this way, the variable series resistance can be calculated for each point. In the other side, the exact value of R_s at V_{oc} is given in Eq. (16) and can be used for verification of the extracted results as follows:

$$R_s^{var}(V_{oc}) = R_s^{oc} \quad (20)$$

Table 1 Different cells and their corresponding processes used

Cells	Active	Layers	Solvents annealed
A	P3HT:C60	Cl-naph:CB	No
B	P3HT:C60	M-naph:CB	No
C	P3HT:C60	ODCB	Yes
D	P3HT:PC61BM	ODCB	No
E	P3HT:C60	ODCB	No

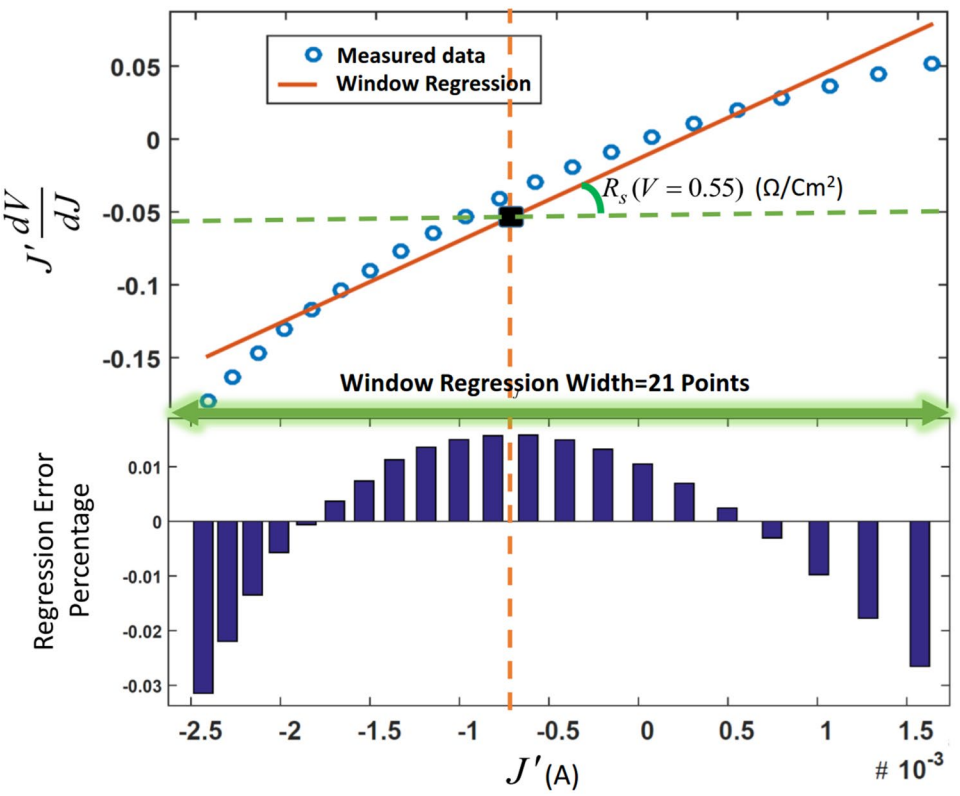

Fig. 4 **a** An example of using the WRA introduced in Eq. (18). **b** The corresponding regression error percentage. In this window the maximum regression error is 0.03%

5 Application to organic solar cells

In this section, our extraction method is applied to the measured J–V characteristics of five BHJ cells based on the blend of P3HT:C60 and P3HT:PC61BM. Figure 2 illustrates structure of these five OSCs.

In these OSCs, PEDOT:PSS and LiF are used as buffer layers and the active layer materials are listed in Table 1. In all cells, P3HT (poly(3-hexylthiophene)) is employed as electron donor polymer and cheap fullerene C60 and [6,6]-phenyl-C61-butyric acid methyl ester (PC61BM) are also used as electron acceptors.

The solvents used are 1-Chloronaphtalene mixed with Chlorobenzene (Cl-naph:CB), 1-Methylnaphtalene mixed with Chlorobenzene (M-naph:CB) and ODCB. The cells A and B are prepared with the two first solvent mixtures. The annealed cell of C (P3HT:C60) and also D and E cells are processed using ODCB solvent. First, the proposed GA method is used to extract J_0, n, R_p, J_{ph} and a constant value R_s^{GA} for all cells variants and the results are presented in Table 2. The OSC A that prepared with Cl-naph:CB has the least series resistance among all other four cells. In comparison with other cells, because the cells' area is constant (0.09 cm^2), it can be infer that cell A has a lower active area series resistance due to larger carrier mobility.

The diode ideality factor (n) is related to types of recombination and quantitatively describes the active layer morphology. One possible explanation could be, a larger n implies more aggregation and larger polymer:fullerene interfacial areas and higher exciton dissociation probability within the active layer [6]. Table 2 shows the biggest n for the variant D (made of P3HT:PC61BM). In fact, solubility of PC61BM in ODCB solvent is much higher than others. The lowest ideality factor of cell B (in Table 2) indicates that this structure behaves more similar to a bilayer OSC. By comparing the FFs of C and E cells (see Fig. 5), annealed and untreated cells processed with ODCB solvent, respectively, indicates performance enhancement by annealing. Also, one can see that the photocurrent improves and the series resistance decreases by annealing. These are mainly due to P3HT recrystallization, which in turn enhances the carrier mobility and improves the charge transport.

The series resistance at maximum power point, higher applied voltages and open circuit voltage is extracted using Eqs. (13), (14) and (16). Table 3 shows these results for the five OSCs under test. From the extraction results it is obvious that the R_s decreases by applied voltage, which is mainly related to the field dependency of the carriers mobility. This has been already confirmed in previous researches [22, 27, 62].

Also, by using relation (18) and the proposed WRA, the voltage dependent series resistances ($R_s(V)$) for all the cells under test can be extracted from J–V characteristics. The results are presented in Fig. 6. The extracted results presented in Fig. 6 show that generally the series resistance decreases by increasing the voltage. These results show a good consistency with the simple approximation model given in Eq. (10). It should be mention that by considering a voltage dependent, the J–V curves predicted by the modified single diode equivalent circuit have a much better

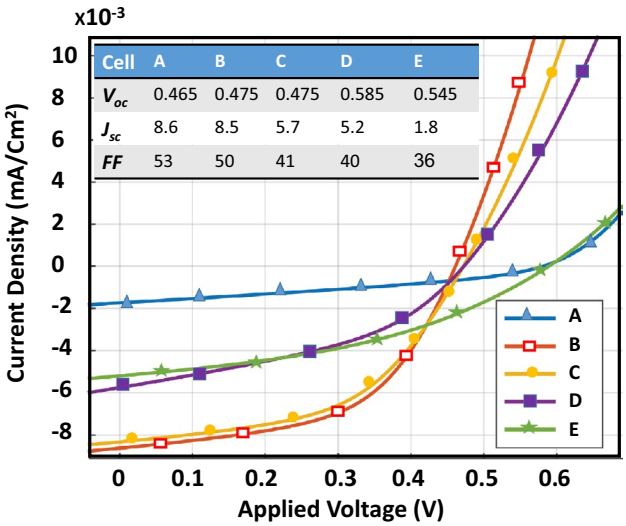

Fig. 5 J–V characteristics of the cells under test

Table 2 Extracted model parameters with the proposed genetic algorithm for all the cells variants

Cells	A	B	C	D	E
$J_0(\mu A)$	1.52	4.4	13	27.4	0.97
n	3.2	2.5	3.3	4.6	3.2
$J_{ph}(mA)$	8.7	8.5	5.9	5.4	1.8
R_p	310	340	194	370	514
R_s	4.5	6.9	6.4	15	6.5
MSE	2.5e−8	1.3e−8	5.3e−9	1e−9	1.1e−7

Table 3 Extracted series resistance from different methods for all the cell variants

$R_s(\frac{\Omega}{Cm^2})$	A	B	C	D	E
R_s^{mp}	47	41	81	68	300
R_s^{oc}	8	10	11	25	30
R_s^{GA}	4.5	6.9	6.4	15	6.5
R_s^{∞}	1.2	2.1	3.3	1.8	4.5

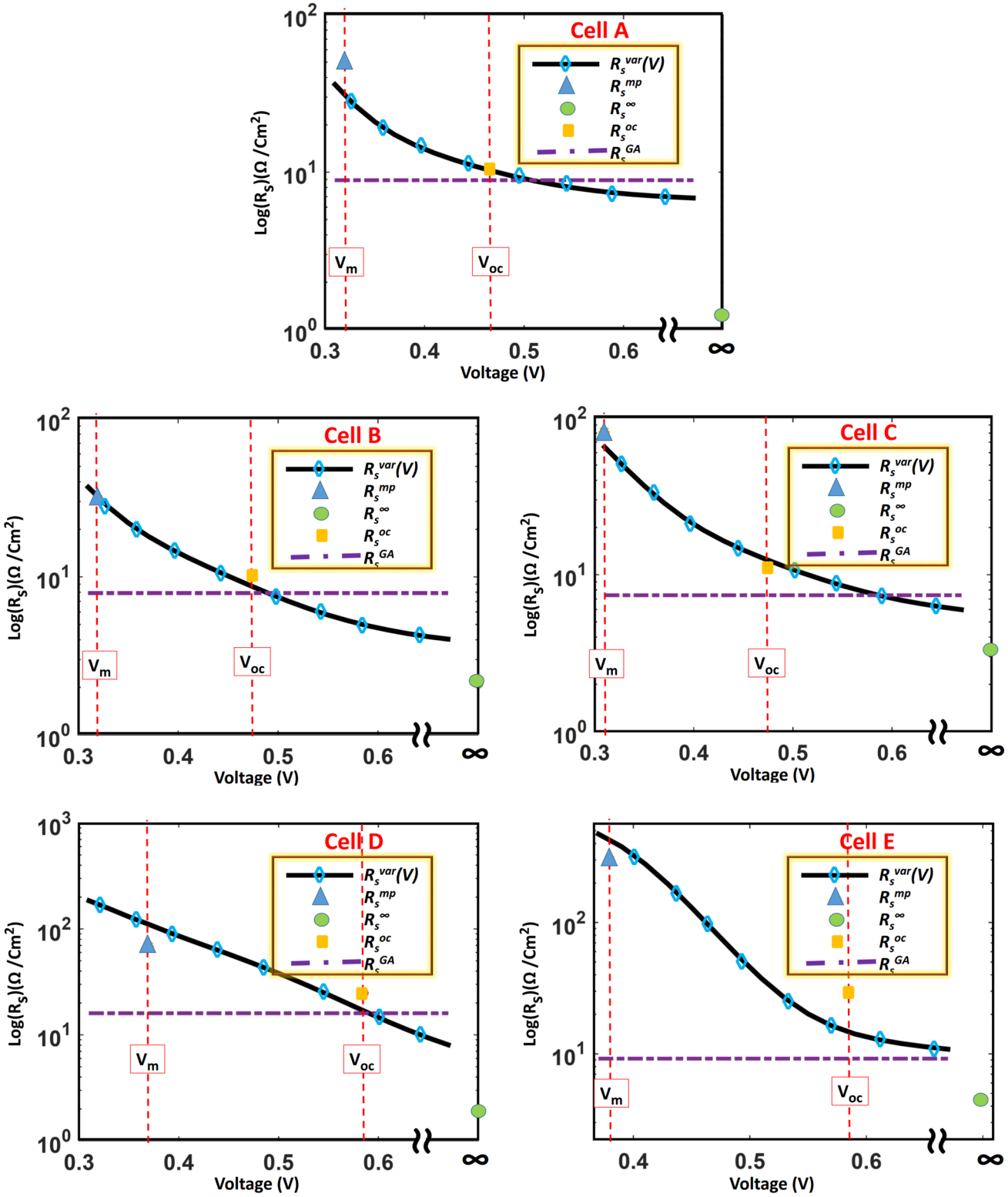

Fig. 6 Extracted voltage dependent series resistances for the cells under test

fitting to the measured J–V characteristics. Table 4 compares the MSE of the fitting process of GA extraction to those of the new WRA approach. For a better comparison, the series resistances extracted using relations (12), (13), (16) and (18) along with the extracted voltage dependent are illustrated in a separate diagram for each cell variant in Fig. 6.

Table 4 MSE for the cells under test considering constant or variable R_s

MSE	*	**	***
A	2.5e−8	2.1e−2	1.5e−10
B	1.3e−8	8.6e−3	1.2e−10
C	5.3e−9	5.7e−4	3.7e−10
D	1e−9	1.0e−2	7.6e−12
E	1.1e−7	6.5e−5	1.3e−11
Average	2e−8	8e−3	1.3e−10

*Fourth quarter of J–V curve only

**First and fourth quarter with constant value of R_s

***First and fourth quarter with variable extracted R_s

A good agreement between the extracted voltage dependent R_s at open circuit point ($R_s^{Var}(V_{oc})$ obtained from WRA) and R_s^{oc} which was calculated from accurate equation of (16) is obtained. The difference between $R_s^{Var}(V_{oc})$ and R_s^{oc} for cell E is mainly related to the limitation in measuring the extremely low current values at V_{oc}. However, it is obvious that the simple dynamic resistance at maximum power point (R_s^{mp} achieved from Eq. (13) is not a very good approximation for the series resistance value at this voltage. In addition, $R_s^{Var}(V_{oc})$ at considerable high applied voltages reduces to a constant value that is a good approximation for the fixed part of the series resistance (R_s^{fix}). On the other hand, since in this region the diode behavior is mainly controlled by its series resistance, the dynamic resistance (R_s^{∞}) is a very good estimation of $R_s^{Var}(\infty)$. That means:

$$R_s^{\infty} = \frac{dV}{dJ}|_{V=\infty} \cong R_s^{fix} \tag{21}$$

Therefore, the final modified equivalent circuit model is similar to that of Fig. 7.

The voltage dependency of R_s is mainly due to the electrical field dependency of mobility of the organic material.

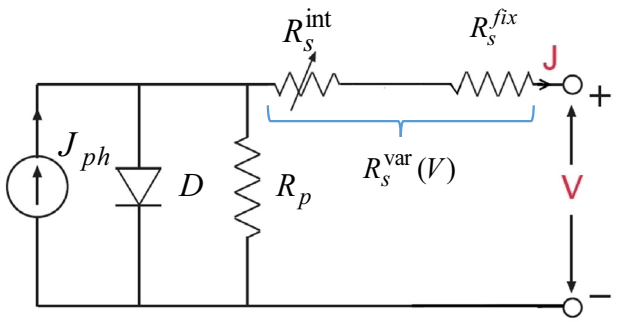

Fig. 7 Extracted voltage dependent series resistances for the cells under test

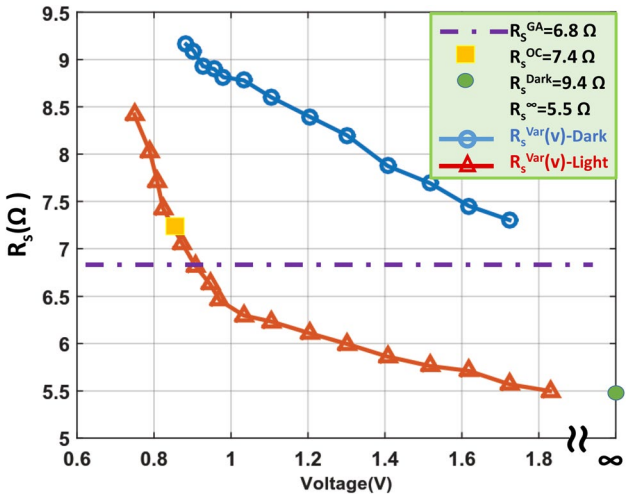

Fig. 8 The extracted series resistances of a typical OSC under dark and light conditions.R_s^{GA} is extracted R_s using GA algorithm in fourth quarter of I–V curve, R_s^{oc} is R_s at open circuit bias, R_s^{dark} is R_s under dark condition at voltages higher than V_{oc} and R_s^{∞} is R_s under illumination at voltages higher V_{oc}

The charge carrier density increases exponentially with voltage, which is reflected in the conductivity (Eq. 8).This can explain the exponential drop in R_s observed in the moderate voltages in Fig. 6. Space charge accumulation also affects the internal electrical field and as a result the series resistance changes. Since the photo generated carriers density is very low in dark condition, the space charge accumulation is decreased and voltage dependency of R_s reduces. In Fig. 8 the extracted series resistances of OSC under dark and light (AMG1.5) conditions are compared.

The series resistances as a functions of voltage are extracted using the proposed algorithm from the measured I–V curves of an OSC with glass/ITO/PEDOT/MEH-PPV: PCBM (1:4)/LiF/Al structure [55]. Although the dark series resistance is higher than that of under illumination, the light R_s shows a stronger nonlinearity behavior versus the applied voltage. For example, for the voltage range of 0.7 V to 1.8 V we have only a 30% variation in the dark R_s against 55% changes in the light R_s. This considerable difference between the dark and light measured series resistances justifies that using the dark R_s instead of the light R_s in PV arrays modeling under illumination is erroneous.

6 Conclusion

In this paper, we proposed an electrical equivalent circuit model for OSCs where its accuracy is highly improved by considering a voltage-dependent series resistance. Using a proposed WRA for this model, the series resistance profile was extracted and compared with the results obtained

by analytical equations at V_{mp}, V_{oc} and high applied voltages. The extracted results confirm reporting a single value R_s of OSC is not generally an accurate approach. Finally, the modified model was applied to measured J–V curves of five different cells, in which the active layers are processed using different materials and solvents. The solvent considerably influenced the active layer crystallinity and its charge carrier mobility, hence, the series resistance is largely affected. Moreover, a voltage dependent series resistance provides a good knowledge about the behavior of the OSC at different applied voltage regions. The proposed model can be used for better understanding the devices physics and to investigate the effects of different parameters including fabrication process parameters, geometry and morphology of the active layer on the cell electrical characteristics.

Acknowledgements This work was supported by Ferdowsi University of Mashhad under Project Nr. of 33469 and by Iran Ministry of Energy under Project Nr. M/145/93. The authors would like to thank Prof. Li in South China University of technology for his helps and supports especially experimental data.

Compliance with ethical standards

Conflict of interest On behalf of all authors, the corresponding author states that there is no conflict of interest.

References

1. Ameri T, Khoram P, Min J, Brabec CJ (2013) Organic ternary solar cells: a review. Adv Mater 25(31):4245–4266. https://doi.org/10.1002/adma.201300623
2. Araujo G, Sanchez E, Marti M (1982) Determination of the two-exponential solar cell equation parameters from empirical data. Solar Cells 5(2):199–204. https://doi.org/10.1016/0379-6787(82)90027-8
3. Blom PW, Mihailetchi VD, Koster LJA, Markov DE (2007) Device physics of polymer: fullerene bulk heterojunction solar cells. Adv Mater 19(12):1551–1566
4. Bouzidi K, Chegaar M, Bouhemadou A (2007) Solar cells parameters evaluation considering the series and shunt resistance. Solar Energy Mater Solar Cells 91(18):1647–1651. https://doi.org/10.1016/j.solmat.2007.05.019
5. Brabec CJ (2004) Organic photovoltaics: technology and market. Solar Energy Mater Solar Cells 83(2):273–292. https://doi.org/10.1016/j.solmat.2004.02.030 The development of organic and polymer photovoltaics
6. Brabec CJ, Durrant JR (2008) Solution-processed organic solar cells. MRS Bull 33(7):670675. https://doi.org/10.1557/mrs2008.138
7. Brenes-Badilla D, Coutinho DJ, Amorim DRB, Faria RM, Salvadori MC (2018) Reversing an S-kink effect caused by interface degradation in organic solar cells through gold ion implantation in the PEDOT:PSS layer. J Appl Phys 123(15):155502. https://doi.org/10.1063/1.5017672
8. Buxton GA, Clarke N (2006) Computer simulation of polymer solar cells. Model Simul Mater Sci Eng 15(2):13
9. Charles JP, Abdelkrim M, Muoy YH, Mialhe P (1981) A practical method of analysis of the current–voltage characteristics of solar cells. Solar Cells 4(2):169–178. https://doi.org/10.1016/0379-6787(81)90067-3
10. Chegaar M, Azzouzi G, Mialhe P (2006) Simple parameter extraction method for illuminated solar cells. Solid-State Electron 50(78):1234–1237. https://doi.org/10.1016/j.sse.2006.05.020
11. Cheknane A, Hilal HS, Djeffal F, Benyoucef B, Charles JP (2008) An equivalent circuit approach to organic solar cell modelling. Microelectron J 39(10):1173–1180. https://doi.org/10.1016/j.mejo.2008.01.053
12. Cheng P, Li G, Zhan X, Yang Y (2018) Next-generation organic photovoltaics based on non-fullerene acceptors. Nat Photon 12(3):131. https://doi.org/10.1038/s41566-018-0104-9
13. Coropceanu V, Cornil J, da Silva Filho DA, Olivier Y, Silbey R, Brdas JL (2007) Charge transport in organic semiconductors. Chem Rev 107(4):926–952
14. de Castro FA, Heier J, Nesch F, Hany R (2010) Origin of the kink in current-density versus voltage curves and efficiency enhancement of polymer-c_{60}heterojunction solar cells. IEEE J Sel Top Quantum Electron 16(6):1690–1699. https://doi.org/10.1109/JSTQE.2010.2040807
15. Driscoll TA, Hale N, Trefethen LN (2014) Chebfun Guide. Pafnuty Publications, Oxford
16. Easwarakhanthan T, Bottin J, Bouhouch I, Boutrit C (1986) Nonlinear minimization algorithm for determining the solar cell parameters with microcomputers. Int J Solar Energy 4(1):1–12. https://doi.org/10.1080/01425918608909835
17. Elumalai NK, Vijila C, Jose R, Ming KZ, Saha A, Ramakrishna S (2013) Simultaneous improvements in power conversion efficiency and operational stability of polymer solar cells by interfacial engineering. Phys Chem Chem Phys 15(43):19057–19064
18. García-Sánchez FJ, Romero B, Lugo-Muñoz DC, Del Pozo G, Arredondo B, Liou JJ, Ortiz-Conde A (2017) Modelling solar cell S-shaped IV characteristics with DC lumped-parameter equivalent circuits a review. Facta Univ Ser Electron Energetics 30(3):327–350. https://doi.org/10.2298/FUEE1703327G
19. Gaur A, Kumar P (2014) An improved circuit model for polymer solar cells. Prog Photovolt Res Appl 22(9):937–948
20. Glatthaar M, Riede M, Keegan N, Sylvester-Hvid K, Zimmermann B, Niggemann M, Hinsch A, Gombert A (2007) Efficiency limiting factors of organic bulk heterojunction solar cells identified by electrical impedance spectroscopy. Solar Energy Mater Solar Cells 91(5):390–393. https://doi.org/10.1016/j.solmat.2006.10.020 Selected papers from the European conference on hybrid and organic solar cells—ECHOS '06
21. Green MA, Emery K, Hishikawa Y, Warta W, Dunlop ED (2016) Solar cell efficiency tables (version 47). Prog Photovolt Res Appl 24(1):3–11. https://doi.org/10.1002/pip.2728
22. Guerrero A, Ripolles-Sanchis T, Boix PP, Garcia-Belmonte G (2012) Series resistance in organic bulk-heterojunction solar devices: modulating carrier transport with fullerene electron traps. Org Electron 13(11):2326–2332. https://doi.org/10.1016/j.orgel.2012.06.043
23. Heitzinger C, Ringhofer C, Selberherr S et al (2007) Finite difference solutions of the nonlinear Schrödinger equation and their conservation of physical quantities. Commun Math Sci 5(4):779–788
24. Irwin MD, Buchholz DB, Hains AW, Chang RPH, Marks TJ (2008) p-type semiconducting nickel oxide as an efficiency-enhancing anode interfacial layer in polymer bulk-heterojunction solar cells. Proc Natl Acad Sci 105(8):2783–2787. https://doi.org/10.1073/pnas.0711990105
25. Jain A, Kapoor A (2005) A new approach to study organic solar cell using lambert W-function. Solar Energy Mater Solar Cells 86(2):197–205. https://doi.org/10.1016/j.solmat.2004.07.004

26. Jin JW, Jung S, Bonnassieux Y, Horowitz G, Stamateri A, Kapnopoulos C, Laskarakis A, Logothetidis S (2016) Universal compact model for organic solar cell. IEEE Trans Electron Dev 63(10):4053–4059
27. Junsangsri P, Lombardi F (2010) Modelling and extracting parameters of organic solar cells. Electron Lett 46(21):1462–1464. https://doi.org/10.1049/el.2010.2232
28. Kim CH, Beliatis MJ, Gandhi KK, Rozanski LJ, Bonnassieux Y, Horowitz G, Silva SRP (2015) Equivalent circuit modeling for a high-performance large-area organic photovoltaic module. IEEE J Photovolt 5(4):1100–1105
29. Kim T, Kim JH, Kang TE, Lee C, Kang H, Shin M, Wang C, Ma B, Jeong U, Kim TS (2015) Flexible, highly efficient all-polymer solar cells. Nat Commun. https://doi.org/10.1038/ncomms9547
30. Koster L, Smits E, Mihailetchi V, Blom P (2005) Device model for the operation of polymer/fullerene bulk heterojunction solar cells. Phys Rev B 72(8):085205
31. Koster LJA, Smits ECP, Mihailetchi VD, Blom PWM (2005) Device model for the operation of polymer/fullerene bulk heterojunction solar cells. Phys Rev B 72:085205. https://doi.org/10.1103/PhysRevB.72.085205
32. Kumar P, Gaur A (2013) Model for the JV characteristics of degraded polymer solar cells. J Appl Phys 113(9):094505
33. Kumar A, Sista S, Yang Y (2009) Dipole induced anomalous S-shape IV curves in polymer solar cells. J Appl Phys 105(9):094512
34. Lan S, Kimoto Y, Fujita K (2017) Necessity of interlayer in tandem organic solar cells composed of a bulk heterojunction unit cell and the equivalent circuit. Mol Cryst Liq Cryst 654(1):249–255. https://doi.org/10.1080/15421406.2017.1358054
35. Masatoshi W, Akio U (1980) Simple method for the determination of series resistance and maximum power of solar cell. Jpn J Appl Phys 19(S2):179
36. Mazhari B (2006) An improved solar cell circuit model for organic solar cells. Solar Energy Mater Solar Cells 90(78):1021–1033. https://doi.org/10.1016/j.solmat.2005.05.017
37. Mialhe P, Khoury A, Charles JP (1984) A review of techniques to determine the series resistance of solar cells. Phys Status Solidi (a) 83(1):403–409. https://doi.org/10.1002/pssa.2210830146
38. Mihailetchi V, Koster L, Hummelen J, Blom P (2004) Photocurrent generation in polymer-fullerene bulk heterojunctions. Phys Rev Lett 93(21):216601
39. Mihailetchi VD, Xie H, de Boer B, Koster LA, Blom PW (2006) Charge transport and photocurrent generation in poly (3hexylthiophene): methanofullerene bulkheterojunction solar cells. Adv Funct Mater 16(5):699–708
40. Müller TC, Pieters BE, Rau U, Kirchartz T (2013) Analysis of the series resistance in pin-type thin-film silicon solar cells. J Appl Phys 113(13):134503. https://doi.org/10.1063/1.4798393
41. Neher D, Kniepert J, Elimelech A, Koster LJA (2016) A new figure of merit for organic solar cells with transport-limited photocurrents. Sci Rep 6:24861. https://doi.org/10.1038/srep24861
42. Ouennoughi Z, Chegaar M (1999) A simpler method for extracting solar cell parameters using the conductance method. Solid-State Electron 43(11):1985–1988. https://doi.org/10.1016/S0038-1101(99)00174-4
43. Prince M (1955) Silicon solar energy converters. J Appl Phys 26(5):534–540
44. Qi B, Wang J (2013) Fill factor in organic solar cells. Phys Chem Chem Phys 15:8972–8982. https://doi.org/10.1039/C3CP51383A
45. Romero B, del Pozo G, Arredondo B (2012) Exact analytical solution of a two diode circuit model for organic solar cells showing S-shape using lambert W-functions. Solar Energy 86(10):3026–3029. https://doi.org/10.1016/j.solener.2012.07.010
46. Romero B, del Pozo G, Arredondo B, Martín-Martín D, Gordoa MPR, Pickering A, Pérez-Rodríguez A, Barrena E, García-Sánchez FJ (2017) S-shaped IV characteristics of organic solar cells: solving mazharis lumped-parameter equivalent circuit model. IEEE Trans Electron Dev 64(11):4622–4627
47. Servaites JD, Yeganeh S, Marks TJ, Ratner MA (2010) Efficiency enhancement in organic photovoltaic cells: consequences of optimizing series resistance. Adv Funct Mater 20(1):97–104. https://doi.org/10.1002/adfm.200901107
48. Servaites JD, Ratner MA, Marks TJ (2011) Organic solar cells: a new look at traditional models. Energy Environ Sci 4:4410–4422. https://doi.org/10.1039/C1EE01663F
49. Sha WEI, Li X, Choy WCH (2014) Breaking the space charge limit in organic solar cells by a novel plasmonic-electrical concept. Sci Rep 4:6236. https://doi.org/10.1038/srep06236
50. Shibayama N, Zhang Y, Satake T, Sugiyama M (2017) Modelling of an equivalent circuit for Cu_2ZnSnS_4- and $Cu_2ZnSnSe_4$-based thin film solar cells. RSC Adv 7(41):25347–25352
51. Singh NS, Amit J, Kapoor A (2013) An exact analytical method for calculating the parameters of a real solar cell using special trans function theory (STFT). Int J Renew Energy Res IJRER 3(1):201–206
52. Slooff LH, Veenstra SC, Kroon JM, Verhees W, Koster LJA, Galagan Y (2014) Describing the light intensity dependence of polymer: fullerene solar cells using an adapted shockley diode model. Phys Chem Chem Phys 16(12):5732–5738. https://doi.org/10.1039/C3CP55293D
53. Small CE, Chen S, Subbiah J, Amb CM, Tsang SW, Lai TH, Reynolds JR, So F (2012) High-efficiency inverted dithienogermole-thienopyrrolodione-based polymer solar cells. Nat Photon 6(2):115–120
54. Turek M (2014) Current and illumination dependent series resistance of solar cells. J Appl Phys 115(14):144503. https://doi.org/10.1063/1.4871017
55. Vanlaeke P, Swinnen A, Haeldermans I, Vanhoyland G, Aernouts T, Cheyns D, Deibel C, DHaen J, Heremans P, Poortmans J, Manca J (2006) P3HT/PCBM bulk heterojunction solar cells: relation between morphology and electro-optical characteristics. Solar Energy Mater Solar Cells 90(14):2150–2158. https://doi.org/10.1016/j.solmat.2006.02.010
56. Wagenpfahl A, Rauh D, Binder M, Deibel C, Dyakonov V (2010) S-shaped current–voltage characteristics of organic solar devices. Phys Rev B 82:115306. https://doi.org/10.1103/PhysRevB.82.115306
57. Warashina M, Ushirokawa A (1980) Simple method for the determination of series resistance and maximum power of solar cell. Jpn J Appl Phys 19(S2):179. https://doi.org/10.7567/JJAPS.19S2.179
58. Wei E, Li X, Choy WC (2014) Breaking the space charge limit in organic solar cells by a novel plasmonic-electrical concept. Sci Rep 4:6236. https://doi.org/10.1038/srep06236
59. Xue J, Uchida S, Rand BP, Forrest SR (2004) 4.2 photovoltaic cells with low series resistances. Appl Phys Lett 84(16):3013–3015. https://doi.org/10.1063/1.1713036
60. Yoon W, Boercker JE, Lumb MP, Placencia D, Foos EE, Tischler JG (2013) Enhanced open-circuit voltage of PBS nanocrystal quantum dot solar cells. Sci Rep 3:2225
61. Zohourian Aboutorabi R, Joodaki M (2014) A tripartite physics-based model for organic solar cells
62. Zohourian Aboutorabi R, Joodaki M, Shahbazi K (2014) In-depth analysis of solvent effects on bulk heterojunction solar cell performance, vol 9137, p 913718. https://doi.org/10.1117/12.2052217